International Conference on More Electric Aircraft
Towards greener aviation
Toulouse, February 7-8, 2024

Concept and Control of a Capacitive Boost Processor for a Permanent Magnet Synchronous Motor

Jean-François Bisson (1), Kamal Al-Haddad (2)
1 : École de technologie supérieure, 1100 Notre-Dame O. Montréal (Québec) H3C 1K3
jean-francois.bisson.1@ens.etsmtl.ca
2 : École de technologie supérieure, kamal.al-haddad@etsmtl.ca

Abstract

This paper proposes a method to increase the power density of a flat-poles permanent magnet synchronous motor (PMSM) by adding the voltage of pre-charged capacitors to the motor phases in addition to the phase voltage of a 3-level PWM inverter. A capacitor being connected in series to each phase of the PMSM, each motor phase becomes a RLC circuit. The outcome of this concept is that the PMSM can be operated at its maximum rated torque over a wide speed range. The pre-charged capacitors have two main effects. First, the voltage boost offered by the pre-charged capacitors opposes the PMSM's Back-EMF, allowing to operate the PMSM in Zero d-axis current (ZDAC) even when the Back-EMF significantly exceeds the DC link voltage, therefore eliminating the need to use the field weakening current control technique. Second, the electrical dynamic of a RLC circuit intrinsically oscillates current and voltage. This supports the inverter in generating AC from a DC source. To pre-charge the capacitors, a converter named the Capacitive Boost Processor (CBP) has been designed. This paper presents the PMSM drive system architecture, the proposed topology of the CBP and the proposed control strategy of the PMSM drive. The simulation results of the proposed system are presented in conclusion.

Introduction

Electrical aviation is currently at its first steps, but in the context of global warming, every step is welcome when it goes towards the reduction of greenhouse gases. The main challenge with electrifying aircrafts is the energy storage. The specific energy density and volumetric energy density of a lithium-ion battery (maximum 954 kJ/kg and 2.49 MJ/L respectively) [1] are still far lower than the jet fuel A-1 (43150 kJ/kg and 34.7 MJ/L respectively) [2] commonly used in aviation nowadays. The second challenge is about the electric motors used in the propulsion of electric aircrafts. Thanks to its superior efficiency and power density [3], the Permanent Magnet Synchronous Motor (PMSM) seems to be the best option for an electric aircraft propulsion system. However, the PMSM generates a Back-EMF which amplitude is directly proportional to rotational speed and opposes the input phase voltage.

As the PMSM speed increases, there is a point where the input phase voltage, typically from a Voltage Source Inverter (VSI) connected to a DC source, is not sufficient to oppose the Back-EMF and operate the PMSM drive with the Maximum Torque per Amp (MTPA) Control Technique. From this point, the field weakening current control technique is typically used, which increases the motor speed at the cost of reducing the torque [4]. Unfortunately, field weakening current control of a PMSM is not a suitable option for aircraft propulsion systems, as the torque load of an aircraft propeller increases with speed. To extend the speed range of MTPA control and therefore delay the field weakening current control, the DC voltage source may be increased using a DC-DC Step-up converter upstream of the VSI [4]-[5]-[11]. This solution has the effect of increasing the power density of the motor by achieving MTPA current control over a wider speed range, but it has drawbacks. First, increasing the DC link voltage upstream of the VSI increases the voltage stress and losses in the VSI components [6]-[7]. Second, the VSI switching at higher DC voltage induces higher phase current Total Harmonic Distortion (THD), which in turns induces more iron losses in the motor [8]. Increasing the switching frequency of the VSI has the effect of reducing the phase current harmonics, but at the cost of increased switching losses [6]-[7]. Third, the additional DC-DC conversion stage brings additional weight and losses.

To benefit from the higher DC link voltage while reducing the phase current THD, a multi-level VSI may be used. A multi-level VSI has the characteristic of reducing the phase current THD in a PMSM compared to a standard 2-level VSI [9]. Another approach for increasing the power density of a PMSM for a given DC link voltage is to connect capacitors in series to

each phase of the PMSM. This experimentation has been performed by K. Lee and J-I Ha [10] and has shown an improvement of the power density of the PMSM.

This paper proposes a converter named the Capacitive Boost Processor (CBP) and its control algorithm. This converter, connected between a VSI and a PMSM, pre-charges capacitors before they are discharged in the PMSM phases. The concept is to add the pre-charged capacitors voltages to the VSI phase voltages to oppose the PMSM back-EMF, therefore increasing its speed range at maximum rated torque. This paper presents the simulation results of the virtual implementation of the system.

1. System Architecture

The proposed PMSM drive system is composed of two fixed DC voltage sources (Vdc/2), a 3-phase 3-Level Neutral Point Clamped (NPC) T-Type VSI, a Capacitive Boost Processor (CBP), a 3-phase PMSM and a control algorithm. The PMSM drives a propeller. Fig. 1 shows a diagram of the system architecture and interfaces, where the black connections represent the high voltage network and the red arrows represent the control signals.

The 3-phase 3-Level NPC T-Type VSI provides to each phase either 0 V, +Vdc/2 or -Vdc/2. The Neutral of the PMSM being connected to the neutral of the inverter, this configuration allows to control the voltage and current in each phase of the motor independently. This configuration has 27 combinations of voltage output and has the capability of providing 0 V, +Vdc/2 or -Vdc/2 simultaneously on each phase of the PMSM. Fig. 2 shows the topology of the selected 3-phase 3-Level VSI, where the black connections represent the high voltage network and the red parameters represent the control signals.

The PMSM is a flat poles PMSM with a wye phase connection configuration, and which has the neutral point accessible. It generates a sinusoidal Back-EMF Ea,b,c as shown in (1.1) to (1.3) where φ_f is the flux linkage in Wb, ω_e is the electrical frequency in rad/sec and θ_e is the rotor electrical angle in rad. The electromagnetic torque equation of the PMSM in the 3-phase model is shown in (2). The PMSM being a flat poles machine, one finds the electromagnetic torque equation in the d-q model as shown in (3). Fig. 3 shows the equivalent electrical circuit of the PMSM.

$$E_a = \varphi_f \cdot \omega_e \cdot \sin(\theta_e) \quad (1.1)$$

$$E_b = \varphi_f \cdot \omega_e \cdot \sin(\theta_e - 2\pi/3) \quad (1.2)$$

$$E_c = \varphi_f \cdot \omega_e \cdot \sin(\theta_e + 2\pi/3) \quad (1.3)$$

$$T = \frac{P_p \cdot (E_a \cdot I_a + E_b \cdot I_b + E_c \cdot I_c)}{\omega_e} \quad (2)$$

$$T = \frac{3}{2} \cdot P_p \cdot \varphi_f \cdot I_q \quad (3)$$

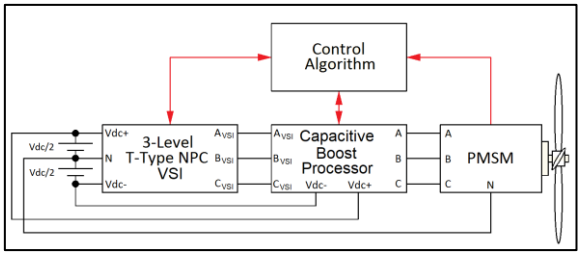

Fig. 1: Proposed PMSM System Drive

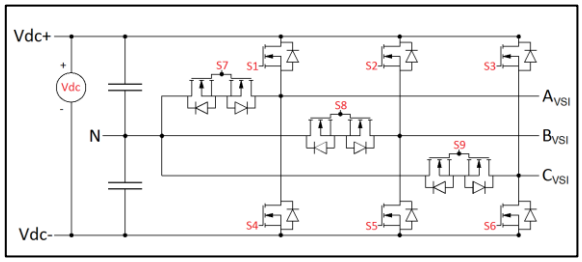

Fig. 2: 3-phase 3-Level NPC T-Type VSI Topology

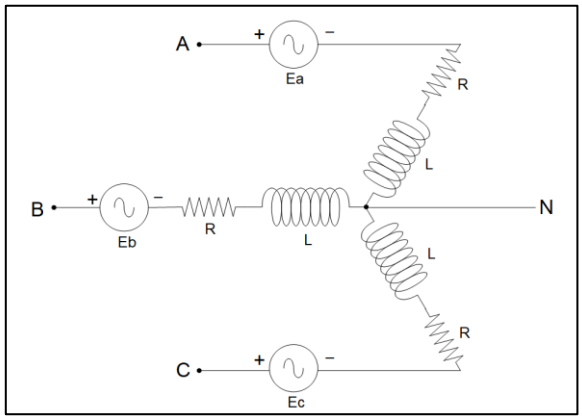

Fig. 3: Equivalent Electrical Circuit of the PMSM

2. Capacitive Boost Power Processor

The purpose of the CBP is to add pre-charged capacitors to the PMSM phases. It is composed of Configurable Capacitor Modules (CCMs) and

Recharge Modules. The proposed topology has four CCMs and one Recharge Module to fit a 3-phase PMSM. However, the CBP architecture is flexible and may fit an electrical machine with any number of phases. The minimum number of CCMs in the CBP is N+1, where N is the number of phases on the electric machine. The minimum number of Recharge Modules is 1, but more can be added for redundancy or to allow charging multiple CCMs at once. In the proposed configuration, three CCMs are discharging through a motor phase while one CCM is recharged through the Recharge Module. The CBP encloses three bi-directional current transducers on each motor phase (IA, IB, IC) and one unidirectional current transducer on the recharge path (IR).

Each CCM is composed of a voltage transducer (VCX), a variable capacitor, and two layers of bidirectional switches: The Phase/Recharge Module Selection (PRMS) switches (AX, BX, CX and RX), and the Capacitor Polarity Selection (CPS) switches (CPSX1 and CPSX2), where “X” takes the ID of any CCM (1 to 4). The PRMS switches connect the capacitor to either a motor phase or the recharge circuit. The PRMS switches come in pairs: one on the VSI side and one on the PMSM side. At all time, only one of the four PRMS switch pairs of a CCM can be closed. The CPS switches make a H-bridge to either bypass the variable capacitor when all four CPSX switches are closed, to isolate the variable capacitor when all four CPSX switches are open, or to set the variable capacitor polarity when only both CPSX1 or both CPSX2 switches are closed. Each bidirectional switch is made of two IGBTs connected in anti-parallel (emitter to emitter). This configuration allows the current in both directions when the gate signal is on, and blocks the current in both directions when the gate signal is off. To simplify the control algorithm, both IGBTs of a bi-directional switch share the same gate control signal. The Variable Capacitor has two possible capacitances: 112 µF or 56 µF. The capacitance of the variable capacitor is set using the bidirectional switch H. The bidirectional switch is made of two IGBTs connected in anti-parallel (emitter to emitter).

The Recharge Module is composed of the recharge inductor (Lr), an IGBT commanded by the gate control signal RON and a freewheeling diode. While the IGBT is commanded ON, the energy from the DC source (Vdc) is added to the recharge inductor/variable capacitor LC circuit. When the RON signal is turned off, the recharge process is completed through the freewheeling diode. The recharge inductor Lr is to benefit from the resonant behaviour of the LC circuit during recharge, allowing to reach a charged capacitor voltage above Vdc. The recharge time is driven by the dynamic of the LC circuit and Lr is sized in order for the natural frequency of the recharge inductor/variable capacitor LC circuit to be at least three times the electrical frequency of the PMSM.

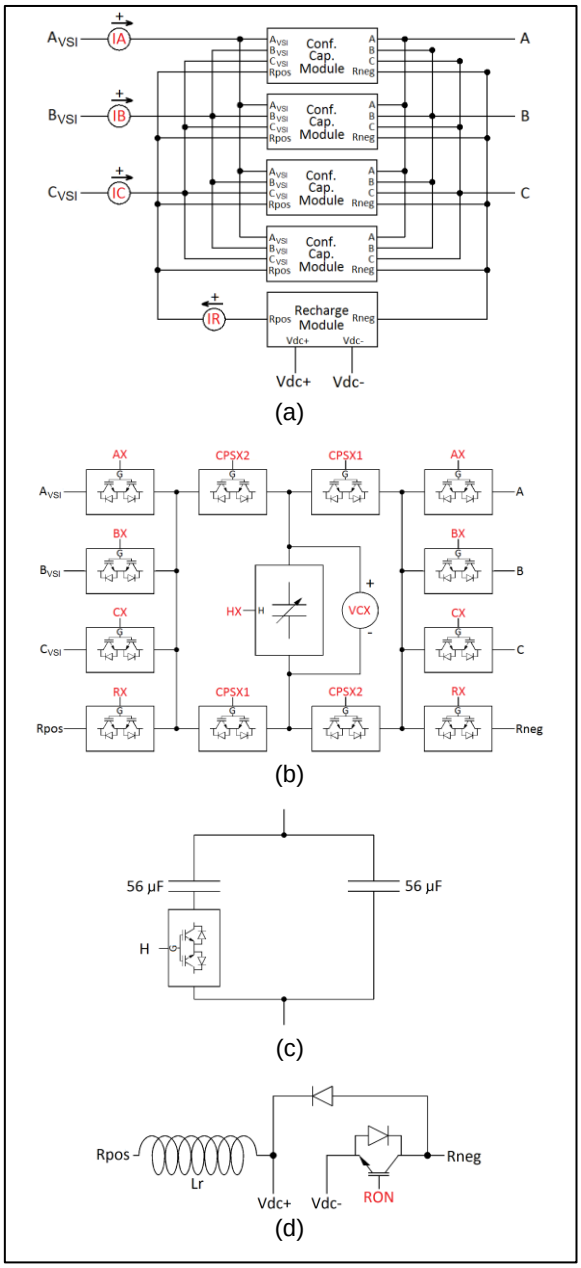

Fig. 4: Topology of the CBP: (a) CBP, (b) CCM, (c) Variable Capacitor, (d) Recharge Module.

3. Mathematical Model

3.1 Semiconductor Losses

The semiconductor devices generate conduction losses in the form of voltage drops across the circuit. The total semiconductor losses in the system consist of the VSI losses ($V_{Loss,VSI}$), the CBP losses ($V_{Loss,CBP}$) and the Recharge Module losses ($V_{Loss,RM}$). Equations (4) to (7) show the equations of the voltage drops across the IGBTs and MOSFETs in forward and reverse current. Equation (8) shows the equation of the forward voltage drop in the Recharge Module diode. Equations (9) and (10) show the equations of the voltage drops across the bidirectional switches. Tables 1 to 3 show the voltage drops in the system components as a function of their state, where IX is any phase current and IR is the recharge current.

$$V_{CE,IGBT} = 0.021 \cdot I + 1.7 \quad (4)$$

$$V_{EC,IGBT} = 0.023 \cdot I + 1.2 \quad (5)$$

$$V_{DS,MOSFET} = 0.1 \cdot I \quad (6)$$

$$V_{SD,MOSFET} = 0.7 \quad (7)$$

$$V_{F,Diode} = 0.018 \cdot I + 0.7 \quad (8)$$

$$V_{switch,IGBT} = V_{CE,IGBT} + V_{EC,IGBT} \quad (9)$$

$$V_{switch,MOSFET} = V_{DS,MOSFET} + V_{SD,MOSFET} \quad (10)$$

VX_{VSI} (V)	IX (A)	$V_{Loss,VSI}$ (V)
0	< 0	$V_{switch,MOSFET}$(IX)
0	> 0	$V_{switch,MOSFET}$(IX)
Vdc/2	< 0	$V_{SD,MOSFET}$
Vdc/2	> 0	$V_{DS,MOSFET}$(IX)
-Vdc/2	< 0	$V_{DS,MOSFET}$(IX)
-Vdc/2	> 0	$V_{SD,MOSFET}$

Table 1: Voltage Drop in the VSI

CBP Mode	$V_{Loss,CBP}$ (V)
Offline	$2 \cdot V_{switch,IGBT}$(IX) + $2 \cdot V_{switch,IGBT}$(IX/2)
Online	$4 \cdot V_{switch,IGBT}$(IX)

Table 2: Voltage Drop in the CBP

RON	V_{RON} (V)	$V_{Loss,RM}$ (V)
0	0	$V_{F,Diode}$(IR)
1	Vdc	$V_{CE,IGBT}$(IR)

Table 3: Voltage Drop in the Recharge Module

3.2 Phase Current

When the CBP is offline, the phase circuit includes the VSI, the CBP in capacitor bypass configuration and the PMSM phase. When in offline mode, the CBP only generates conduction losses through the switches and does not provide any capacitive contribution. Equation (11) shows the transfer function of the phase current when the CBP is offline. When the CBP is online, the phase circuit includes the VSI, the CBP and the PMSM phase. Equation (12) shows the transfer function of the phase current when the CBP is online. IX is the phase current of any phase, VX_{VSI} is the VSI output voltage of any phase, Ex is the Back-EMF of any phase, V_{CX0} is the variable capacitor's initial voltage, C is the CMM capacitance and $V_{Loss,X}$ is the sum of the semi-conductors voltage drops across the phase circuit.

$$IX = \frac{(VX_{VSI} - Ex - V_{Loss,X})}{L \cdot s + R} \quad (11)$$

$$IX = \frac{(VX_{VSI} - Ex + V_{C_X0} - V_{Loss,X}) \cdot C \cdot s}{L \cdot C \cdot s^2 + R \cdot C \cdot s + 1} \quad (12)$$

$$V_{Loss,X} = V_{Loss,VSI} + V_{Loss,CBP} \quad (13)$$

3.3 Recharge Circuit

The recharge current goes through the recharge circuit and the CBP. Equation (14) shows the transfer function of the recharge current, where $V_{Loss,R}$ (15) is the voltage drop across the semiconductors of the recharge circuit, C is the CMM capacitance and V_{RON} is the recharge circuit input voltage.

$$IR = \frac{(V_{RON} + V_{C_X0} - V_{Loss,R}) \cdot C \cdot s}{Lr \cdot C \cdot s^2 + R_{Lr} \cdot C \cdot s + 1} \quad (14)$$

$$V_{Loss,R} = V_{Loss,RM} + V_{Loss,CBPP} \quad (15)$$

3.4 Mechanical

In the mechanical model, the electromagnetic torque is transferred into rotor speed and position using the transfer functions of (16), (17) where J is the rotor inertia. The motor load (T_{load}) is the aerodynamic load of the propeller, which increases as a function of speed square, as shown in (18).

$$\omega_e = \frac{P_p \cdot (T - T_{load})}{J \cdot s} \quad (16)$$

$$\theta_e = \frac{\omega_e}{s} \quad (17)$$

$$T_{load} = 1.8885 \cdot 10^{-6} \cdot \omega_e^2 \quad (18)$$

4. Control Algorithm

The objective of the control algorithm is to control the PMSM rotor speed at 6500 rpm. Fig. 5 shows the architecture of the control algorithm, including the control blocks and the dataflow between the blocks (in red). The “Sensors” block does the analog to digital conversion of the sensors signals. The “VSI Control” block converts the voltage commands from the Field Oriented Control (FOC) into VSI switching commands. The “Switches Command” block makes the digital Boolean signal conversion to analog commands to the gate drivers. The “FOC”, “Main Sequencer” and “Capacitor Module Control” blocks are further explained below.

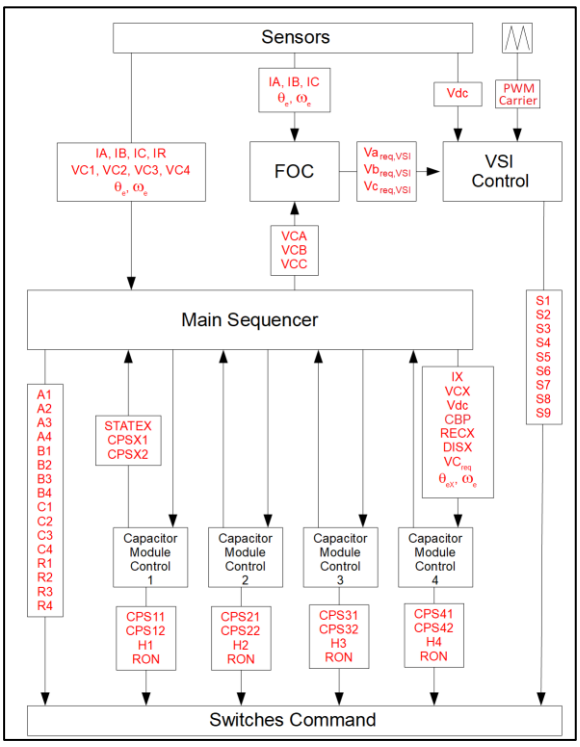

Fig. 5: Architecture of the Control Algorithm

4.1 Field Oriented Control (FOC)

The first step of the FOC is a closed loop control of the motor speed. This is done by a PI controller which outputs a torque request as a function of rotor speed error, then a q-axis current request (Iq_{req}) as shown in Fig. 6. The PMSM drive is controlled using the Zero d-axis current (ZDAC) control method as shown in Fig. 7. D-axis and q-axis currents are calculated using the Park transform at (19), and three-phase voltage commands are calculated using the inverse Park transform in (20). However, the outputs of (20) are not directly used as the voltage commands to the inverter. As shown in (21), real time capacitor voltages are subtracted from the voltage requests of (20) to generate a sinusoidal voltage profile at the PMSM’s phase terminals. The three-phase voltage commands to the inverter are those from (21).

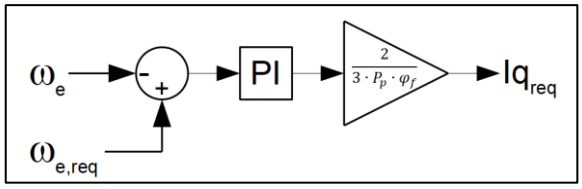

Fig. 6: PMSM Rotor Speed Controller

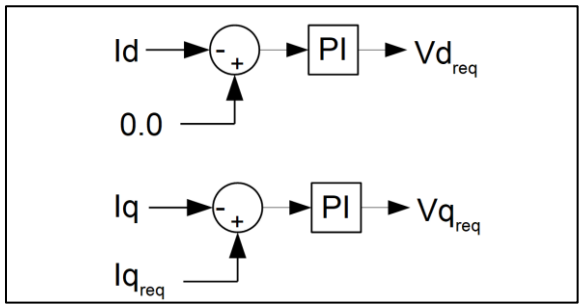

Fig. 7: ZDAC d-q Axis Current Controller

$$\begin{bmatrix} Id \\ Iq \end{bmatrix} = \frac{2}{3} \cdot \begin{bmatrix} \cos(\theta_e) & \sin(\theta_e) \\ -\sin(\theta_e) & \cos(\theta_e) \end{bmatrix} \times \begin{bmatrix} 1 & -\frac{1}{2} & -\frac{1}{2} \\ 0 & \frac{\sqrt{3}}{2} & -\frac{\sqrt{3}}{2} \end{bmatrix} \times \begin{bmatrix} IA \\ IB \\ IC \end{bmatrix} \quad (19)$$

$$\begin{bmatrix} VA_{req} \\ VB_{req} \\ VC_{req} \end{bmatrix} = \begin{bmatrix} 1 & 0 \\ -\frac{1}{2} & \frac{\sqrt{3}}{2} \\ -\frac{1}{2} & -\frac{\sqrt{3}}{2} \end{bmatrix} \times \begin{bmatrix} \cos(\theta_e) & -\sin(\theta_e) \\ \sin(\theta_e) & \cos(\theta_e) \end{bmatrix} \times \begin{bmatrix} Vd_{req} \\ Vq_{req} \end{bmatrix} \quad (20)$$

$$\begin{bmatrix} VA_{req,VSI} \\ VB_{req,VSI} \\ VC_{req,VSI} \end{bmatrix} = \begin{bmatrix} VA_{req} \\ VB_{req} \\ VC_{req} \end{bmatrix} - \begin{bmatrix} VCA \\ VCB \\ VCC \end{bmatrix} \quad (21)$$

4.2 Main Sequencer

The Main sequencer oversees the control of the CBP. It performs the subtasks enumerated below.

- Activation of the CBP: At speeds below 2700 rpm, the CBP is in Offline mode. The CBP goes in Online mode when the PMSM rotor speed reaches the speed threshold of 2700 rpm. Once this speed threshold is reached, the Main Sequencer informs the CCMs that the CBP is online by setting the “CBP”

Boolean signal to 1.

- Scheduling of the Recharge Module connection: This sub-task schedules the Recharge Module to recharge each CCM in alternance. This subtask monitors the state of each CCM and when a CCM is in “Discharged” state and the Recharge Module is available, it connects the discharged CCM to the Recharge Module using the “RX” bidirectional switches. It ensures that only one CCM is commanded to be recharged at a time. This subtask sets the Boolean signal “RECX” to 1 to inform the CCM X that its state can transition from “Discharged” to “Recharging”, where “X” takes the ID of any CCM.
- Scheduling of the Motor Phases connection: This subtask monitors the state of each CCM and when a CCM is in “Recharged” state, it waits for a motor phase d-axis (zero Back-EMF) crossing to enable the discharge of the CCM in the selected PMSM phase. Every time a PMSM phase crosses the d-axis, a charged CCM is connected to the PMSM phase using the “AX”, “BX” or “CX” bidirectional switches. This subtask ensures that only one PMSM phase is connected to a CCM at a time. This subtask sets the Boolean signal “DISX” to 1 to inform the CCM X that its state can transition from “Recharged” to “Discharging”, where X takes the ID of any CCM.
- Calculation of the Capacitor Voltage Request: This subtask calculates the Capacitor Voltage Request VC_{req}. The Capacitor Voltage Request is the target voltage of the CCMs when in “Recharged” state. The purpose of the CCM voltage is to oppose the PMSM Back-EMF. The Capacitor Voltage Request is the amplitude of the PMSM Back-EMF as shown in (22).
- Multiplexing of the Electrical Rotor Angle: This subtask calculates the Electrical Rotor Angle θ_{eX} from the point of view of the different CCMs. As a maximum of one PRMS switch is closed per CCM at a time, the matrix operation at (23) sets θ_{eX} as a function of the PMSM phase connected to the CCM, where X takes the ID of any CCM.
- Multiplexing of the Current Data: This subtask calculates the current from the point of view of the different CCMs. The matrix operation at (24) sets IX as a function of the PMSM phase connected to the CCM, where X takes the ID of any CCM.
- Multiplexing of Voltage Data: This subtask calculates the CCM voltage from the point of view of the PMSM phases. To be used in (21), the Capacitor Voltages need to be matched to the PMSM phase they are connected to. The first matrix operation sets the polarity of CCM as a function of the CPS switches, as shown in (25.1). The second matrix operation sets VCX as a function of the PRMS switches and CCM polarity, as shown in (25.2), where X takes the ID of any PMSM phase.

$$VC_{req} = \varphi_f \cdot \omega_e \tag{22}$$

$$\begin{bmatrix}\theta_{e1}\\ \theta_{e2}\\ \theta_{e3}\\ \theta_{e4}\end{bmatrix} = \begin{bmatrix}A1 & B1 & C1 & R1\\ A2 & B2 & C2 & R2\\ A3 & B3 & C3 & R3\\ A4 & B4 & C4 & R4\end{bmatrix} \times \begin{bmatrix}\theta_e\\ \theta_e - 2\pi/3\\ \theta_e + 2\pi/3\\ 0\end{bmatrix} \tag{23}$$

$$\begin{bmatrix}I1\\ I2\\ I3\\ I4\end{bmatrix} = \begin{bmatrix}A1 & B1 & C1 & R1\\ A2 & B2 & C2 & R2\\ A3 & B3 & C3 & R3\\ A4 & B4 & C4 & R4\end{bmatrix} \times \begin{bmatrix}IA\\ IB\\ IC\\ IR\end{bmatrix} \tag{24}$$

$$[sign1 \quad sign2 \quad sign3 \quad sign4] = [-1 \quad 1] \times \begin{bmatrix}CPS11 & CPS21 & CPS31 & CPS41\\ CPS12 & CPS22 & CPS32 & CPS42\end{bmatrix} \tag{25.1}$$

$$\begin{bmatrix}VCA\\ VCB\\ VCC\\ 0\end{bmatrix} = \begin{bmatrix}A1 & A2 & A3 & A4\\ B1 & B2 & B3 & B4\\ C1 & C2 & C3 & C4\\ 0 & 0 & 0 & 0\end{bmatrix} \times \begin{bmatrix}sign1 & 0 & 0 & 0\\ 0 & sign2 & 0 & 0\\ 0 & 0 & sign3 & 0\\ 0 & 0 & 0 & sign4\end{bmatrix} \times \begin{bmatrix}VC1\\ VC2\\ VC3\\ VC4\end{bmatrix} \tag{25.2}$$

4.3 Capacitor Module Control

The CCM host the Capacitor Module Control. The Capacitor Module Control is identical in each CCM. It performs the subtasks enumerated below.

- CCM State Machine: The CCM has four states: Discharged, Recharging, Recharged and Discharging. The transitions to Recharging and to Discharging are triggered by the RECX and DISX signals from the Main Sequencer. The trigger to determine that the discharge cycle is done (DIS_DONE) is based on the Electrical Rotor Angle θ_{eX} from the point of view of the CCM. When θ_{eX} gets close to the d-axis zero crossing, the CCM state machine declares the discharge cycle as done. The trigger to determine that the recharge cycle is done (REC_DONE) is based on the recharge current IR. When the recharge current drops to zero, the CCM state machine declares the recharge cycle as done. See Fig. 8 for a schematic of the CCM State

Machine.

- CPS Switches control: When the CBP is offline (CBP signal from the Main Sequencer is false), sets both CPS switches to closed to bypass the variable capacitor. When the CCM State is either Recharged or Discharged, sets both CPS switches to open to isolate the capacitor voltage, waiting for the Recharging or Discharging State. When entering the Recharging State, sets the CPS switches to connect the positive capacitor terminal to the Rneg terminal of the Recharge Module to benefit from the resonant dynamic during the recharge cycle. When entering the Discharging State, sets the CPS switches in order for the CCM voltage to oppose the Back-EMF.
- Capacitance Setting: The Capacitor Module Control sets the capacitance of the Variable Capacitor. When the PMSM speed exceeds 4548 rpm, the HX switch is commanded open and the variable capacitor transitions from 112 μF to 56 μF. This operation is performed when the CCM State is Discharged.
- Recharge Cycle Management: The objective of the Recharge Cycle is to recharge the CCM to the desired voltage before it is discharged in a PMSM phase. To do so, the Capacitor Module Control sets RON = 1 to provide energy from the DC voltage source to the recharge process, or sets RON = 0 to complete the recharge process in freewheeling. Because the recharge cycle is completed in freewheeling, the CCM voltage keep on increasing even if RON is commanded off. A predictive capacitor voltage control sub-algorithm, based on energy, is presented in Fig. 9. The sub-algorithm determines the initial capacitor energy (Einit) and the target capacitor energy (Ereq). The difference between the target capacitor energy and the initial capacitor energy is the energy input request (Ein,req). The energy input (Ein) is the integration of the measured input power, which is the raw input power minus the losses.

5. Simulation Results

The System has been modeled with Matlab/Simulink. The simulated operating condition is a propeller run-up from stop to 6500 rpm, which is the desired operating speed. The simulation has been performed at a fixed sample time of 10^{-6} second and using the Runge-Kutta solver. The simulation parameters are described in Table 4.

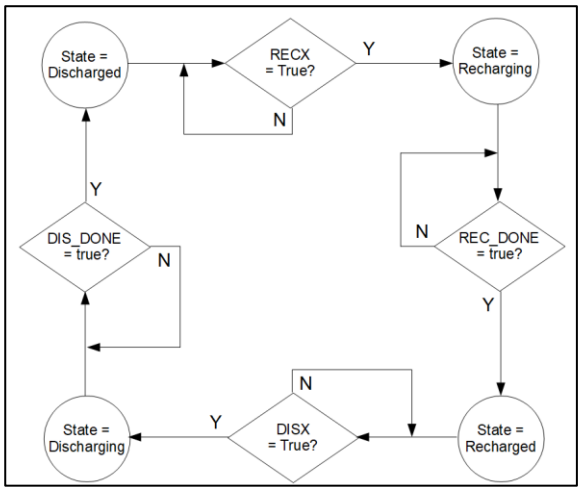

Fig. 8: CCM State Machine

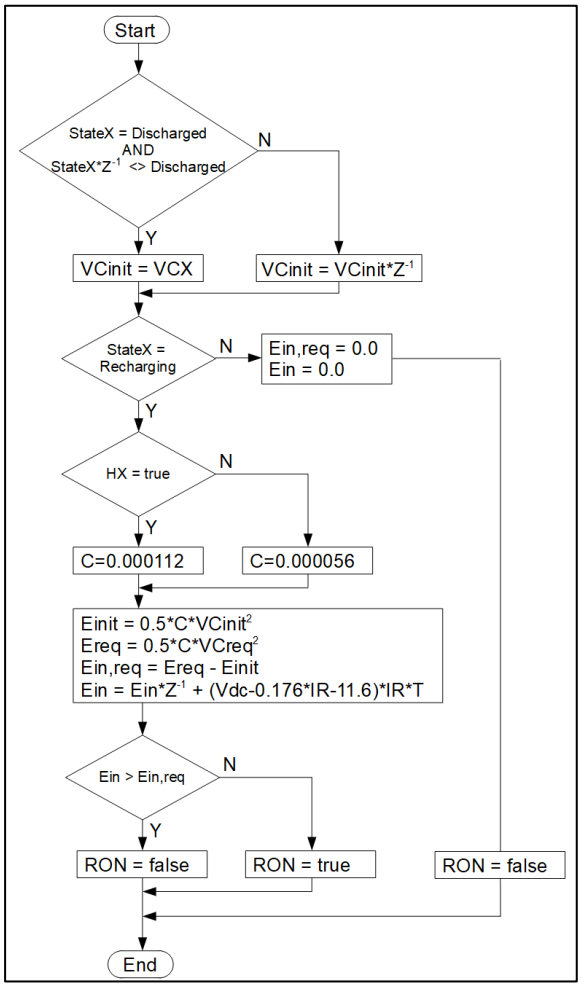

Fig. 9: CCM Predictive Capacitor Voltage Control Sub-Algorithm

Symbol	Definition	Value
φ_f	PMSM Flux Linkage (Wb)	0.161815
P_P	Number of PMSM Pole Pairs	4
Vdc	DC Link Voltage (V)	320
R	PMSM Phase Resistance (Ω)	0.5
L	PMSM Phase Inductance (H)	0.00347
R_{Lr}	Recharge Module Resistance (Ω)	0.002
Lr	Recharge Module Inductance (H)	0.00033
J	Rotor Inertia (kg.m^2)	0.09

Table 4: Simulation Parameters

5.1 PMSM Simulation Results

From the simulation results shown in Fig. 10, one can observe that the nominal power is achieved around 2000 rpm, where the PMSM torque starts decreasing due to the increasing Back-EMF. This is expected as below 2700 rpm, the CBP is offline and therefore does not add the capacitors voltages to the PMSM phases. When the CBP is activated, one can observe that the PMSM torque overshoots the maximum continuous rating of 15.6 N.m. This is due to the FOC PI controller integrators which accumulated the q-axis current error since the q-axis current dropped starting at 2000 rpm. Once the CBP is activated, the PI controller catches-up and the PMSM torque is maintained at the maximum continuous rating. The capacitance shift from 112 μF to 56 μF is smooth from the PMSM point of view. This transition can be observed around t = 3.5 seconds. The proposed system achieves the maximum continuous rated torque over the whole speed range, until the run-up is completed. Once the run-up is completed, the control algorithm proposed in this paper successfully controls the PMSM speed at 6500 rpm and torque at 14 N.m. Looking at Fig. 11, one can observe that the ZDAC control technique is effective throughout the whole speed range. Looking at Fig. 12, one can observe that the combined inverter and capacitor voltages are sufficient to oppose the Back-EMF and achieve the desired phase current. Looking at Fig. 13, one can observe that the profile of the phase current is sinusoidal with low current harmonics. Table 5 shows the PMSM torque and speed properties in steady state.

Parameter	Value
Mean Torque (N.m)	14.0
Torque Fluctuations (N.m)	1.2 p-p
Mean Speed (rpm)	6501
Speed Fluctuations (rpm)	0.1 p-p

Table 5: Steady State Torque and Speed Properties

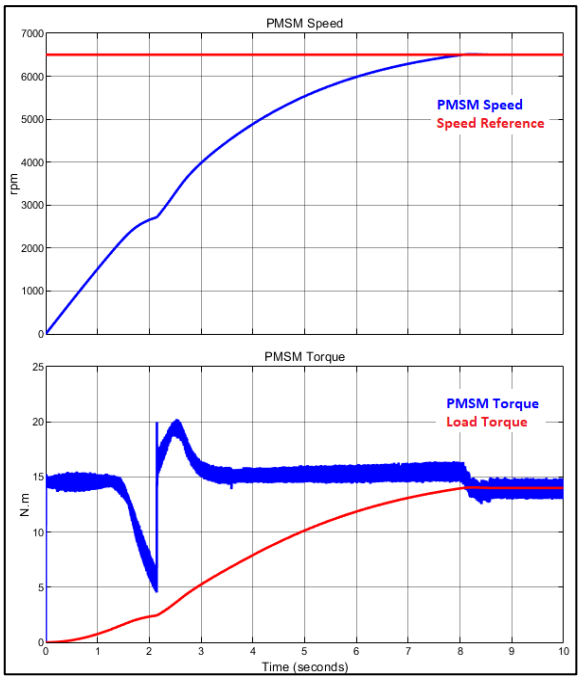

Fig. 10: PMSM Torque and Speed during Run-Up

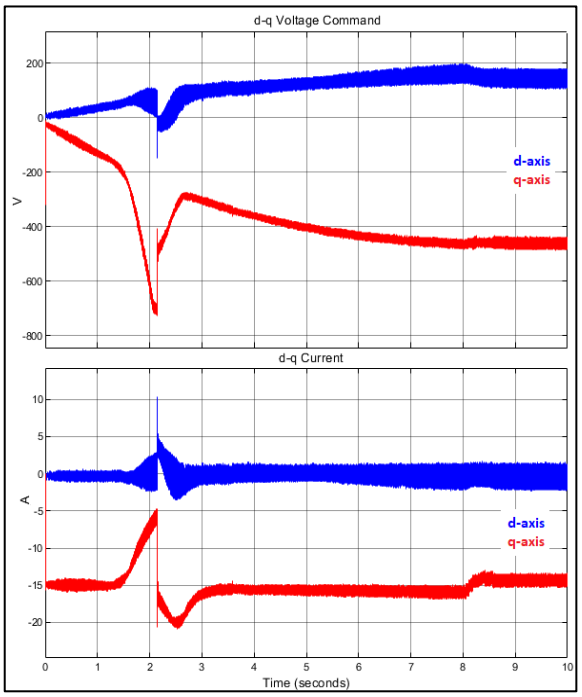

Fig. 11: d-q Axis Phase Voltage Command and Phase Current during Run-up

5.2 CBP Simulation Results

From the simulation results shown in Fig. 14, one can observe that the control algorithm successfully manages the different switches of the CBP to schedule the recharge cycles and discharge cycles. Fig. 14 also shows that the capacitor successfully goes through the recharge and discharge cycles. The PRMS switches are controlled such that only one pair of switches is activated at a time. The CPS switches are controlled such that the capacitor polarity is properly set for the intended usage. Fig. 15 shows the electrical behavior of the Recharge Module, where it can be observed that the control algorithm successfully schedules the recharge cycle of the CCMs by setting RON until the desired amount of energy has been injected in the capacitors. Fig. 16 shows the effectiveness of the energy-based Predictive Capacitor Voltage control sub-algorithm, where is can be observed that the recharged capacitor voltage matches the capacitor voltage request, especially when the CCMs are configured to 56 μF.

6. A Note on Safety and Reliability

Aircraft propulsion systems are amongst the most regulated and safety critical airworthy systems. Their design ensures that the failure rates of the critical components are extremely low, and that even if those critical components fail, degraded operation modes and backup systems ensure that the aircraft can continue to operate safely until landing.

Safety margins per design, redundancy, quality control, Failure Mode Effect Analysis (FMEA), Fault Tree Analysis (FTA), trend monitoring and preventive maintenance are examples of means used by the industry to improve the safety of their products. This paper proposes a system which is at its early conceptual phase, and does not assess the airworthiness potential of the concept. However, a preliminary high-level evaluation of the CBP shows that no single failure point can lead to a complete loss of propulsion power.

The proposed concept has been designed with a modular architecture in which two types of modules are used: Configurable Capacitor Modules (CCM) and Recharge Modules. The system proposed in this paper has five modules in total: 4 CCMs and one Recharge Module. The effect of any of those five modules failing (total disconnection of a CCM or total disconnection of the Recharge Module) would result in a loss of boost

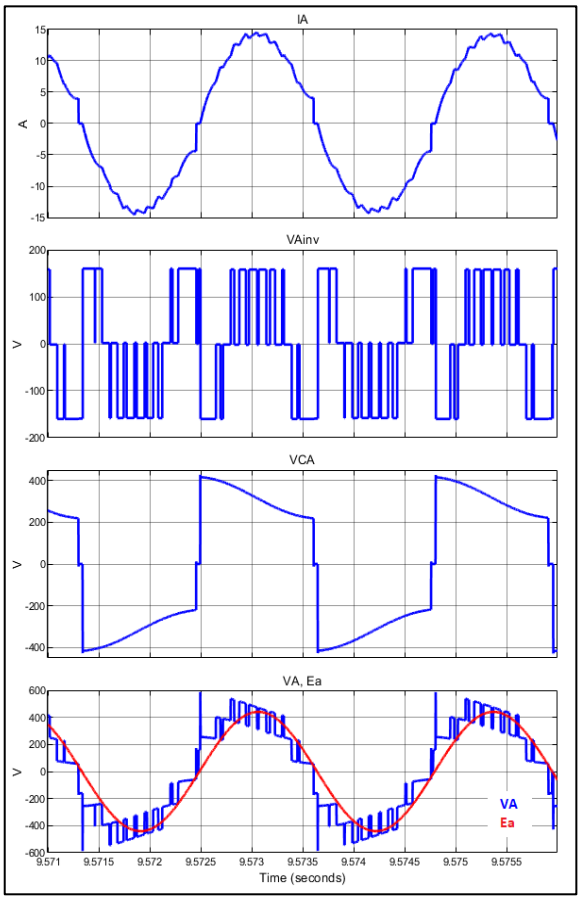

Fig. 12: Phase A Current, VSI Phase A Output Voltage, Phase A CCM Voltage and PMSM Phase A Voltage at 6500 rpm and 14 N.m.

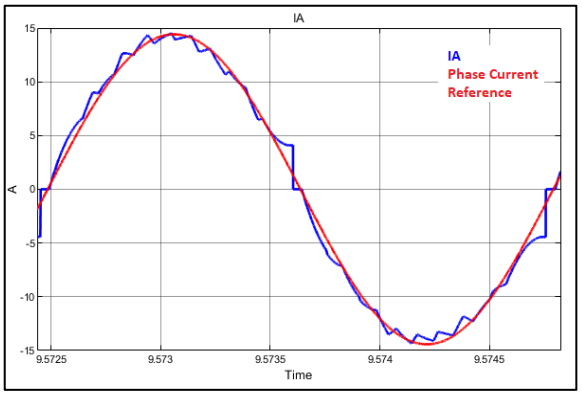

Fig. 13: Phase A Current and Sinusoidal Phase Current Reference at 6500 rpm and 14 N.m.

functionality and the PMSM operating at nominal power, where the PMSM power source would be the DC link through the VSI. In this degraded mode, any three remaining CCM would be configured as a pass-through (capacitor bypass), each CCM linking a VSI phase to a PMSM phase. To result in a total loss of propulsion, two PRMS bidirectional switches need to fail in short circuit mode in the same CCM and on the same side (either the VSI side of the PMSM side).

The severity of the operating conditions of the IGBTs, especially the thermal stresses due to repetitive heating and cooling, accelerate their failure modes [12]. The proposed concept makes a mild use of the semiconductors. As shown in Table 6, the switching frequency of the PRMS, CPS and RON switches is low, and their switching currents are low. Also, adding the capacitor boost voltage downstream of the VSI reduces the voltage stress on the VSI semiconductors comparatively with a voltage boost converter upstream of the VSI, therefore reducing the VSI severity of use.

Finally, the modular architecture of the CBP allows to add a CCM and/or a Recharge Module to the system for redundancy and additional reliability. Use of each CCM and/or Recharge Module during operation would allow to detect dormant failures.

Switch	Switching Freq. (Hz)	Turn-on Current (A)	Turn-Off Current (A)
AX, BX, CX	217	0.0	~4.5
RX	650	0.0	0.0
CPSX1	650	0.0	~4.5
CPSX2	650	0.0	~4.5
RON	2600	0.0	~180.0

Table 6: Switching Frequencies and Switching Currents of the CBP switches at 6500 rpm and 14 N.m.

Conclusions

This paper proposes a preliminary concept of a PMSM drive which includes a capacitor-based phase voltage booster module, herein referred as the Capacitive Boost Processor (CBP). The CBP being connected between the VSI and the PMSM, the VSI voltage stresses and losses are not different to what they would be at nominal power. This proposed drive successfully achieves steady state operation of a PMSM driving a propeller at 6500 rpm and 14 N.m. For the given DC link voltage, the CBP allows to increase

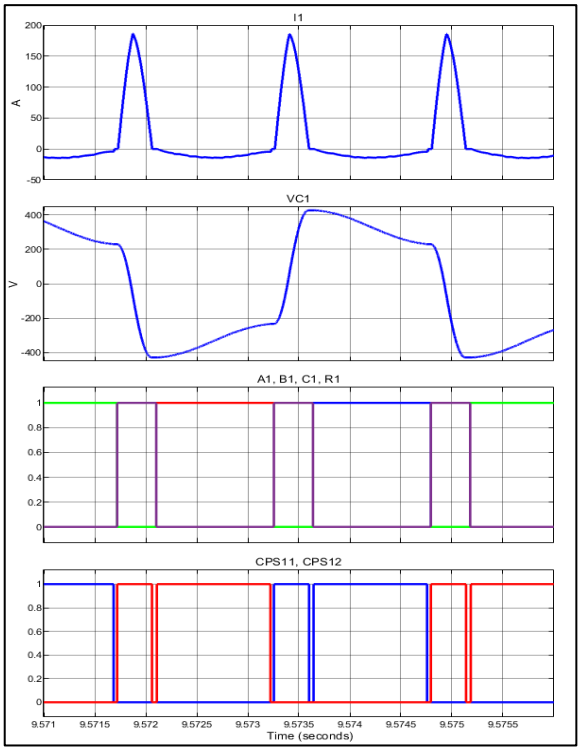

Fig. 14: CCM 1 Current, Voltage, PRMS and CPS

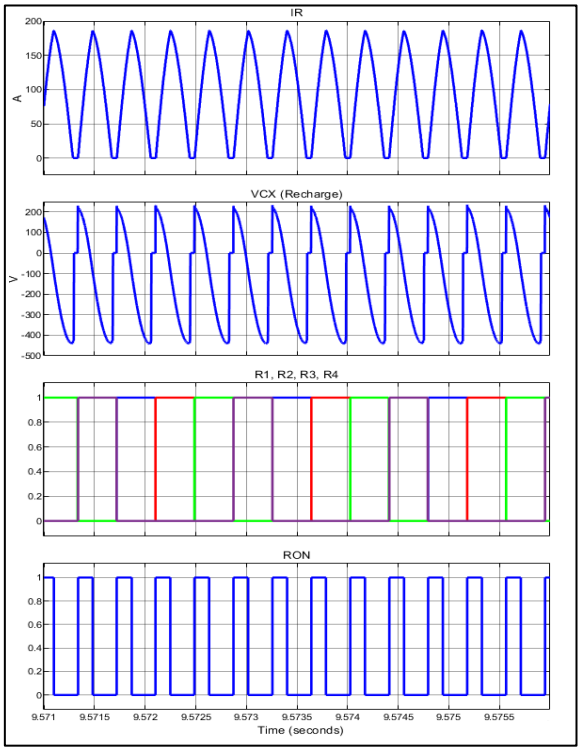

Fig. 15: Recharge Module Operation at 6500 rpm and 14 N.m.

the power of the PMSM to 325% of nominal power, while generating low phase current harmonics. This concept brings the equivalent of turbo-compression for electric motors, which could be fit for electric aircraft propulsion systems, and in particular electric ducted fan engines.

From the simulation results, one can conclude that a functional virtual concept has been developed. The next papers will include an in-depth safety and reliability analysis, and a comparative performance analysis (system level power density and efficiency) with a state-of-the-art technology.

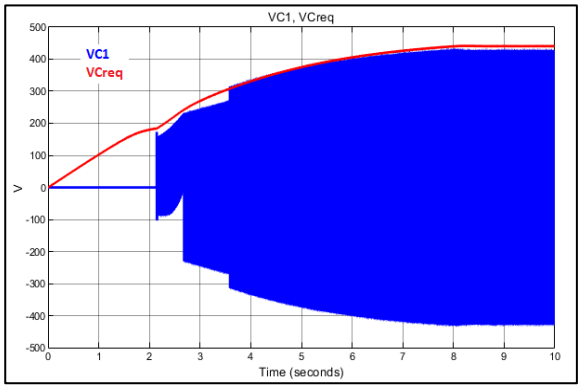

Fig. 16: Recharged VC1 Voltage and VCreq

References

1 Lithium-ion battery (2023, March 12). In Wikipedia. https://en.wikipedia.org/wiki/Lithium-ion_battery.
2 Jet fuel (2023, March 12). In Wikipedia. https://en.wikipedia.org/wiki/Jet_fuel.
3 T. Finken et al, Comparison and design of different electrical machine types regarding their applicability in hybrid electrical vehicles, 18th International Conference on Electrical Machines, 2008, pp. 1-5.
4 K. Yamamoto et al, Comparison between flux weakening and PWM inverter with voltage booster for permanent magnet synchronous motor drive, Proceedings of the Power Conversion Conference-Osaka, 2002, Vol.1, pp. 161-166.
5 D. Tekgun et al, A modular three-phase buck-boost motor drive topology, 2020 6th International Conference on Electric Power and Energy Conversion Systems (EPECS), 2020, pp. 130-135.
6 X. Yu et al, Temperature-related MOSFET power loss modeiling and optimization for DC-DC converter, 2013 Twenty-Eighth Annual IEEE Applied Power Electronics Conference and Exposition (APEC), 2013, pp. 2788-2792.
7 Z. Chen et al, Power losses in two- and three-level three phase photovoltaic inverters equipped with IGBTs, 2012 15th International Conference on Electrical Machines and Systems (ICEMS), 2012, pp. 1-6.
8 K. Yamazaki et al, Harmonic Loss and Torque Analysis of High-Speed Induction Motors, IEEE Transactions on Industry Applications, 2012, Vol.48, pp. 933-941.
9 D. Liang et al, Evaluation of high-speed permanent magnet synchronous machine drive with three-level and two-level inverter, 2015 IEEE International Electric Machines & Drives Conference (IEMDC), 2015, pp. 1586-1592.
10 K. Lee et al, Power Capability Improvement of Interior Permanent Magnet Synchronous Motor Drives Using Capacitive Network, 2019 IEEE Applied Power Electronics Conference and Exposition (APEC), 2019, pp. 2597-2602.
11 R. Wang et al, PMSM driving system design for electric vehicle applications based on bi-directional quasi-z-source inverter, 2018 13th IEEE Conference in Industrial Electronics and Applications (ICIEA), 2018, pp. 1733-1738.
12 A. Abuelnaga et al, A Review on IGBT Module Failure Modes and Lifetime Testing, IEEE Access, 2021, Vol.9, pp. 9643-9663.